Experimental test of universal conductance fluctuations by means of wave-chaotic microwave cavities

Sameer Hemmady,[1,2,3,4] James Hart,[1] Xing Zheng,[1] Thomas M. Antonsen, Jr.,[1,2,3] Edward Ott,[1,2,3] and Steven M. Anlage[1,2,4]
[1]*Department of Physics, University of Maryland, College Park, Maryland 20742-4111, USA*
[2]*Department of Electrical and Computer Engineering, University of Maryland, College Park, Maryland 20742-3285, USA*
[3]*Institute for Research in Electronics and Applied Physics, University of Maryland, College Park, Maryland 20742-3511, USA*
[4]*Center for Superconductivity Research, University of Maryland, College Park, Maryland 20742-4111, USA*
(Received 26 June 2006; published 15 November 2006)

The mathematical equivalence of the time-independent Schrödinger equation and the Helmholtz equation is exploited to provide a means of studying universal conductance fluctuations in ballistic chaotic mesoscopic systems using a two-dimensional microwave cavity. The classically chaotic ray trajectories within a suitably shaped microwave cavity play a role analogous to that of the chaotic dynamics of noninteracting electron transport through a ballistic quantum dot in the absence of thermal fluctuations. The microwave cavity is coupled through two single-mode ports and the effect of nonideal coupling between the ports and cavity is removed by a previously developed method based on the measured radiation impedance matrix. The Landauer-Büttiker formalism is applied to obtain the conductance of a corresponding mesoscopic quantum-dot device. We find good agreement for the probability density functions of the experimentally derived surrogate conductance, as well as its mean and variance, with the theoretical predictions of Brouwer and Beenakker. We also observe a linear relation between the quantum dephasing parameter and the cavity ohmic loss parameter.

DOI: 10.1103/PhysRevB.74.195326 PACS number(s): 73.23.−b

I. INTRODUCTION

Much attention has been focused on the problem of mesoscopic transport through a quantum dot in which a two-dimensional electron gas system contained within an arbitrarily shaped potential-well boundary is connected to two electron reservoirs through leads—the source (s) and drain (d). Recently it has been possible to fabricate quantum dots with low impurity content where the elastic mean free paths of the enclosed electrons are typically much larger than the physical size of the dot.[1] Electron transport through such "ballistic dots" is governed by elastic collisions off the enclosing potential-well boundaries. It has been observed that the terminal conductance of such dots, defined as $\hat{G}=I_s/(V_s-V_d)$ where I_s is the source current flowing into the dot and (V_s-V_d) is the potential difference between these two leads, exhibits strong, reproducible fluctuations on the order of the quantum of conductance $(G_0=e^2/h)$ (Refs. 2–4). These fluctuations arise from quantum-interference effects due to the phase-coherent electron transport within such dots and have been explained using the hypothesis that the fluctuations are governed by random matrix theory.[5] Similar universal conductance fluctuations (UCF) were previously observed in other systems such as quasi-one-dimensional metal wires.[6–8]

In a quantum dot, this phase coherence is partly lost by opening the system to the outside world during the process of measurement of the conductance. Quantum phase decoherence (dephasing) can also be induced due to the presence of impurities within the dot, thermal fluctuations, or electron-electron interactions, all of which lead to more classical properties for electron transport.[9] Significant theoretical and experimental effort has been devoted to studying the dephasing of the transport electrons in quantum dots.[10–12] One class of theoretical dephasing models utilizes a "fictitious voltage probe (ϕ)" attached to the dot that has a number of channels (modes) N_ϕ, each of which contains a tunnel barrier with transmission probability Γ_ϕ for the electrons that enter the channel from the dot. Electrons that enter one of the modes of this probe are re-injected into the dot with a phase that is uncorrelated with their initial phase, and there is no net current through the fictitious probe. An alternative model of electron transport employs a uniform imaginary term in the electron potential,[13,14] leading to loss of probability density with time. It was shown in Ref. 15 that, as far as the conductance is concerned, these two models yield equivalent predictions in the limit when the number of channels in the dephasing lead $N_\phi\to\infty$ and $\Gamma_\phi\to 0$, with the product $\gamma=N_\phi\Gamma_\phi$ remaining finite ("the locally weak absorbing limit").[16] A similar idea exists for describing ohmic losses in the microwave cavity in terms of nonideally coupled "parasitic channels."[17] Since the ohmic losses in the microwave cavity are to good approximation uniformly distributed, we can make use of the equivalence of the imaginary potential and voltage leads models mentioned above to relate the dephasing parameter γ employed by electron-transport theory[15] to the loss parameter of our microwave cavity $[k^2/(\Delta k_n^2 Q)]$ (Refs. 18–21). Here, $k=2\pi f/c$ is the wave number for the incoming frequency f and Δk_n^2 is the mean-spacing of the adjacent eigenvalues of the Helmholtz operator, ∇^2+k^2, as predicted by the Weyl formula[22] for the closed system. The quantity Q represents the loaded quality factor of the cavity. Using the prescription outlined by Ref. 15 we can directly determine the analog of conductance for the microwave cavity and make detailed comparisons of data to theory.

We use an electromagnetic analog of a quantum dot in the form of a two-dimensional chaotic microwave resonator.[23] In the case of a cavity thin in one dimension, Maxwell's equations reduce to a two-dimensional scalar Helmholtz equation. Owing to the analogy between the scalar Helmholtz equation

and the Schrödinger equation,[24] the chaotic microwave cavity is an ideal surrogate for a ballistic quantum dot without the complicating effects of thermal fluctuations,[4] Coulomb interactions, or impurities. The microwave cavity is driven by two ports, both of which support a single propagating mode and are analogous to the source and drain leads in the quantum dot. The microwave analog permits detailed measurements of the eigenvalues,[25–27] eigenfunctions,[28–32] scattering and reaction matrices,[19–21,33–36] in a system where every detail of the potential and the coupling channels can be controlled.

Adopting a variant of the Landaeur-Büttiker formalism, the normalized conductance ($G=\hat{G}/2G_o$) can be expressed in terms of the scattering matrix $\overleftrightarrow{s}=\begin{pmatrix} s_{11} s_{12} \\ s_{21} s_{22} \end{pmatrix}$ of a chaotic cavity when the leads (ports) are perfectly coupled to the cavity,[37] i.e.,

$$G = |s_{12}|^2 + \frac{(1-|s_{11}|^2-|s_{12}|^2)(1-|s_{22}|^2-|s_{21}|^2)}{2-|s_{11}|^2-|s_{12}|^2-|s_{21}|^2-|s_{22}|^2}, \quad (1)$$

where the first term describes the direct (phase coherent) transport through the microwave cavity and corresponds to the conductance of the quantum dot due to the electrons that did not enter the fictitious voltage probe. The second term is a correction that describes the conductance due to the electrons that are re-injected into the dot from the phase-breaking fictitious voltage probe, thereby ensuring particle conservation in the voltage-probe model.[15]

In the time-reversal symmetric case with single-mode leads, Ref. 15 has shown that as γ increases the probability density function of G [i.e., $P(G;\gamma)$] becomes more and more sharply peaked around the classical value of $G=1/2$. In the limit of large γ, an asymptotic analytic expression for $P(G;\gamma)$ is predicted to be (Ref. 15),

$$P(G;\gamma) = \frac{1}{2}\gamma(1+|x|-x)e^{-|x|} \quad \text{with } x = 2\gamma(G-1/2). \quad (2)$$

This yields a large-γ asymptotic expression for the mean and variance of G which are predicted to be (Ref. 15),

$$\langle G \rangle = \frac{1}{2} - \frac{1}{2\gamma} + O(\gamma^{-2}), \quad (3)$$

$$\mathrm{var}(G) = \frac{3}{4\gamma^2} + O(\gamma^{-3}). \quad (4)$$

This paper is divided into the following sections. In Sec. II, we present a brief description of the experimental setup and data analysis. In Sec. III, we present the experimental results by first examining the relation between the dephasing parameter (γ) and the cavity loss parameter $[k^2/(\Delta k_n^2 Q)]$. Section IV then uncovers the PDFs of the experimentally determined universal conductance fluctuations for increasing values of γ and compares them with predictions from Ref. 15 and random matrix theory. In Sec. V, we experimentally test the predictions from Ref. 15 for the mean and variance of these universal conductance fluctuation PDFs as a function of γ. Finally, Sec. VI concludes this paper with a summary of our experimental findings and its implications.

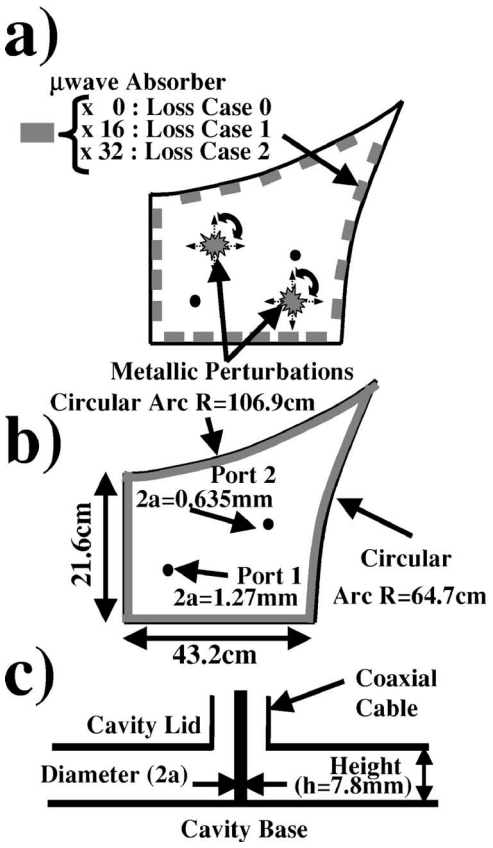

FIG. 1. (a) Top view of quarter-bow-tie microwave cavity used for the experimental "cavity case." The two perturbations are shown as the gray shapes. The small, gray, uniformly spaced rectangles lining the side walls of the cavity represent 2 cm-long strips of microwave absorber which are used to control the loss in the cavity. (loss case 0: 0 strips, loss case 1: 16 strips, loss case 2: 32 strips). (b) The implementation of the experimental "radiation case" is shown. The gray lining on the side walls is a homogenous layer of microwave absorber about 2 mm thick. The physical dimensions of the cavity are shown in the schematic. The approximate locations of the two driving ports are also shown. (c) Cross-section view of both driving ports inside the cavity. The cavity is 7.87 mm in depth. The diameter of the inner conductor is 2a (=1.27 mm for Port 1; =0.635 mm for Port 2).

II. EXPERIMENTAL SETUP AND DATA ANALYSIS

The microwave cavity under study is a metallic, air-filled, quarter bow-tie shaped chaotic resonator [Fig. 1(a)] which is quasi-two-dimensional for frequencies below 19.05 GHz. The cavity is driven by two single-mode, coaxial transmission lines whose inner conductor [diameters 2a=1.27 mm for Port 1, 2a=0.635 mm for Port 2 as shown in Fig. 1(b)] extends from the top plate of the cavity and makes contact with the bottom plate [shown as a schematic in Fig. 1(c)]. An ensemble data set of one hundred similar cavities with different internal field configurations is generated by rotating and translating two metallic perturbations, each of which are

roughly the size of a wavelength at 5 GHz [gray jagged shapes in Fig. 1(a)], within the cavity volume. This approach of configuration averaging to approximate a pure ensemble average is similar in principle to deforming the shape of the potential-well boundary of a quantum dot as performed by (Ref. 4) although in our case the volume of the system is fixed. In addition to the intrinsic ohmic loss in the cavity, the degree of loss can be further increased in a controlled manner by partially lining the inner side walls of the cavity with 2 cm-long strips of microwave absorber having uniform spacing. This results in three experimental loss cases—loss case 0: no absorbing strips, loss case 1: 16 absorbing strips, loss case 2: 32 absorbing strips. A fourth experimental loss case is created by placing the loss case 0 cavity in a bath of dry ice (solid CO_2 at −78.5 °C). This has the effect of slightly increasing the loss case 0 cavity Q value (by ~10%). We refer to this case as the "dry-ice case." A more detailed explanation of our experimental setup and data analysis can be found in Ref. 21.

For our investigation, we generate a large ensemble of 2×2 cavity scattering matrices ($\overleftrightarrow{S}$) for the four loss cases through measurements for different configurations of the perturbers at many frequencies in a range from 3 to 18 GHz (covering about 800 modes of the cavity). Using the "radiation impedance" approach[18–21] [Fig. 1(b)], the nonideal coupling details of the two ports are removed to yield an ensemble of normalized 2×2 scattering matrices ($\overleftrightarrow{s}$) from which the conductance statistics are derived using Eq. (1).

Prior to reporting results for different "data sets" where each data set corresponds to one of our four loss cases and a frequency range typically spanning about 1 GHz, we estimate the value of γ for each data set. We derive an analytic expression for the mean value of the absorption probability $\langle T\rangle$ in terms of γ from Eq. (17a) of Ref. 15,

$$\langle T_1\rangle = \langle T_2\rangle = \langle T\rangle = \frac{1}{4\gamma}\{e^{-\gamma}[4(e^{\gamma}-\gamma-1)+4e^{\gamma}(2e^{\gamma}-2-\gamma(2+\gamma))\xi(-\gamma)-2e^{\gamma/2}[e^{\gamma}(2+\gamma(\gamma-2))-2]\xi(-\gamma/2)]\}, \quad (5)$$

where $\xi(z)=-\int_{-z}^{\infty}\frac{e^{-t}}{t}dt$ is the exponential integral function. Here $1-T_1$ and $1-T_2$ are the eigenvalues of $\overleftrightarrow{s}\overleftrightarrow{s}^{\dagger}$, and $\langle T_1\rangle = \langle T_2\rangle$ since the joint PDF of T_1 and T_2 [Eq. (17a) of Ref. 15] is symmetrically distributed. The inset in Fig. 2 shows the relation between $\langle T\rangle$ and γ on a semilogarithmic plot (gray curve). By determining the value of $\langle T\rangle$ from the measured data set, Eq. (5) then uniquely determines the corresponding value of $\gamma(\equiv\gamma_{\langle T\rangle})$.

To determine the cavity loss parameter $k^2/(\Delta k_n^2 Q)$ for our data sets, we employ one of two procedures. For data sets with $k^2/(\Delta k_n^2 Q)\leqslant 5$, we numerically generate marginal PDFs of the real and imaginary parts of the normalized impedance $[\overleftrightarrow{z}=(\overleftrightarrow{s}+\overleftrightarrow{1})(\overleftrightarrow{s}-\overleftrightarrow{1})^{-1}]$ eigenvalues using random-matrix Monte Carlo simulations with square matrices of size $N=1000$, and the value of $k^2/(\Delta k_n^2 Q)$ in the simulations ranges from 0.1 to 5 in steps of 0.1. We determine the variance (σ^2) of these numerically generated PDFs and fit it to a polynomial function $\sigma^2=\Theta[k^2/(\Delta k_n^2 Q)]$ of high order. We then determine the variances of the real and imaginary parts of each experimental data set and solve the inverse polynomial function $k^2/(\Delta k_n^2 Q)=\Theta^{-1}(\sigma^2)$ to obtain a unique estimate of $k^2/(\Delta k_n^2 Q)$ corresponding to each data set. For data sets with $k^2/(\Delta k_n^2 Q)>5$, we use the relation $\sigma^2=\frac{1}{\pi[k^2/(\Delta k_n^2 Q)]}$ (Refs. 18, 21, and 38) which has been validated experimentally in Ref. 19.

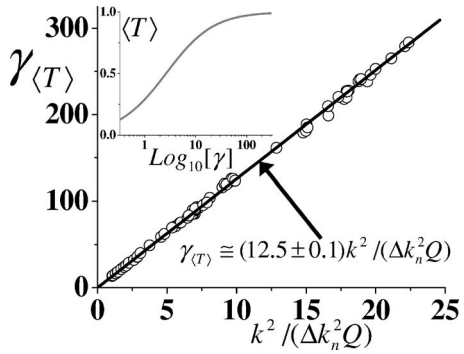

FIG. 2. The relation between the experimentally determined value for $\gamma_{\langle T\rangle}$ and $k^2/(\Delta k_n^2 Q)$ corresponding to each 1 GHz wide data set over the frequency range 3 to 18 GHz for the different cavity loss cases—0, 1, and 2, is shown as the black circles. A linear fit (black line) yields the empirical expression $\gamma_{\langle T\rangle}=(12.5\pm0.1)k^2/(\Delta k_n^2 Q)$. Inset: The relation between $\langle T\rangle$ and γ as expressed in Eq. (5) is shown as the gray curve on a semilogarithmic scale.

III. RELATIONSHIP BETWEEN THE DEPHASING PARAMETER (γ) AND THE CAVITY LOSS PARAMETER [$k^2/(\Delta k_n^2 Q)$]

We begin by examining the relationship between the estimated dephasing parameter $\gamma_{\langle T\rangle}$ and the estimated cavity loss parameter $k^2/(\Delta k_n^2 Q)$. By employing a sliding frequency window 1 GHz wide that runs over each of the three loss cases—0, 1, 2, from 3 to 18 GHz, we estimate the value of $\gamma_{\langle T\rangle}$ and the corresponding value of $k^2/(\Delta k_n^2 Q)$ for each window. The comparison is shown as the black circles in Fig. 2. A linear fit (black line in Fig. 2) yields the empirical expression $\gamma_{\langle T\rangle}=(12.5\pm0.1)k^2/(\Delta k_n^2 Q)$ for about 70 points with values for $\gamma_{\langle T\rangle}$ ranging from about 11 to about 300. By comparing the Poynting theorem for the electromagnetic cavity with the continuity equation for the probability density in the quantum system,[39] we find $\gamma=4\pi k^2/(\Delta k_n^2 Q)$, with $4\pi=12.56\cdots$. This result can be considered an empirical confirmation of the proposed equivalence of the imaginary potential (uniform volume losses) and dephasing lead models in the limit considered in Ref. 15. The 1 GHz width of our sliding window was chosen to be large enough to overcome the effects of short-ray paths (which are not removed by only configuration averaging[18,21]), but at the same time small enough that the cavity losses can be assumed to be approximately constant over this frequency range.

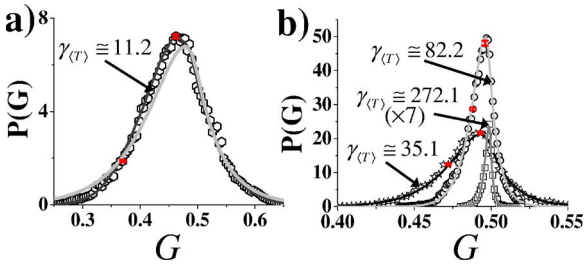

FIG. 3. (Color online) (a) PDFs for the normalized conductance $P(G;\gamma)$ obtained from a chaotic cavity for the dry-ice case: 4.1–4.7 GHz (hexagons) $(k^2/(\Delta k_n^2 Q)=0.9\pm0.1;\gamma_{\langle T\rangle}=11.2\pm0.1)$ and in (b) loss case 0: 16.8–17.6 GHz (stars) $(k^2/(\Delta k_n^2 Q)=2.8\pm0.1;\gamma_{\langle T\rangle}=35.1\pm0.1)$; loss case 1: 8.3–9.5 GHz (circles) $(k^2/(\Delta k_n^2 Q)=6.6\pm0.1;\gamma_{\langle T\rangle}=82.2\pm0.1)$, and loss case 2: 16.8–17.6 GHz (squares) $(k^2/(\Delta k_n^2 Q)=21.7\pm0.1;\gamma_{\langle T\rangle}=272.1\pm0.1)$. The red (dark gray) error bars, which are roughly the size of the symbols, are indicative of the typical statistical binning error in the experimentally determined normalized conductance PDFs. The solid curves [light gray in (a); black, light gray and gray in (b)] are obtained from Eq. (2) and correspond to γ values of 11.2, 35.1, 82.2, and 272.1, respectively. The dark-gray curve in (a) is obtained from random matrix Monte Carlo simulation corresponding to a γ value of 11.2.

IV. UNCOVERING THE UNIVERSAL CONDUCTANCE FLUCTUATION PDFs

In Fig. 3, the experimentally obtained histogram approximation (symbols) to the probability density functions (PDFs) of the normalized conductance $[P(G;\gamma)]$ derived from the normalized scattering matrix $\overleftrightarrow{s}$ and Eq. (1) is shown for four cavity data sets. The solid curves [light gray in Fig. 3(a); black, light gray, and gray in Fig. 3(b)] are the asymptotic analytic expression for $P(G,\gamma)$ [Eq. (2)] with values of γ that correspond to the estimated $\gamma_{\langle T\rangle}$ values obtained from the four cavity data sets. The dark gray solid curve in Fig. 3(a) is a random matrix Monte Carlo simulation for values of $\gamma_{\langle T\rangle}$ corresponding to the data set in Fig. 3(a). The red (dark gray) error bars, which are roughly the size of the symbols in Fig. 3, are representative of the typical statistical binning error of the experimental histograms and show that the agreement between the data (shown by the symbols) and the theoretical predictions (shown by the solid curves) improves as the value of $\gamma_{\langle T\rangle}$ increases. This is to be expected as Eq. (2) is valid only in the high dephasing limit ($\gamma \gg 1$). Similar good agreement between the data and Eq. (2) is obtained for all of the ~40 data sets that we examined in which the frequency ranges and cavity loss cases resulted in the $\gamma_{\langle T\rangle}$ parameter greater than ~18.

In order to bring out the universal scaling behavior of the $P(G;\gamma)$ distributions [Eq. (2)] and also to test that these distributions remain strictly non-Gaussian for increasing values of γ (as predicted by Ref. 15), we rescale the $P(G;\gamma)$ distributions by plotting $\mathrm{Log}_{10}\left[\frac{P(G;\gamma)}{\gamma}\right]$ versus $x=2\gamma(G-1/2)$ in Fig. 4 for three representative data sets (shown as the symbols) with $\gamma_{\langle T\rangle}$ ranging from about 56 to about 220. We observe that the three data sets roughly fall on top of each other. The solid black curve is the theoretical prediction, Eq. (2) which is in good agreement with the data. We observe some deviation of the symbols from the theoretical curve near $x \cong +2$. This is attributed to the lack of adequate statistics in the tails of the experimentally determined histogram approximations to the probability density functions of the conductance. Overall, for values of x ranging from −4 to +2, the agreement is qualitatively good and applies over other data sets where $\gamma_{\langle T\rangle}$ ranges from about 18 to about 330. The asymmetric (nonparabolic) nature of the experimental data, represented by the symbols, confirms that the experimentally obtained $P(G;\gamma)$ remains strictly non-Gaussian and negatively skewed even for large values of γ as predicted by Ref. 15.

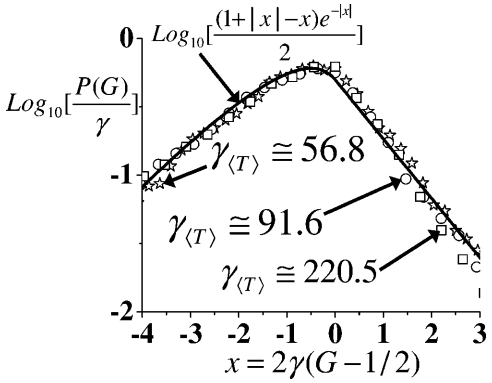

FIG. 4. The universal scaling behavior of the conductance distributions is shown. The vertical axis represents $\mathrm{Log}_{10}\left[\frac{P(G,\gamma)}{\gamma}\right]$ with the corresponding $x=2\gamma(G-1/2)$ along the horizontal axis for three representative data sets consisting of loss case 1: 5.01–6.08 GHz (stars) $(k^2/(\Delta k_n^2 Q)=4.5\pm0.1;\gamma_{\langle T\rangle}=56.6\pm0.1)$; loss case 1: 13.6–14.6 GHz (circles) $(k^2/(\Delta k_n^2 Q)=7.3\pm0.1;\gamma_{\langle T\rangle}=91.6\pm0.1)$, and loss case 2: 13.6–14.6 GHz (squares) $(k^2/(\Delta k_n^2 Q)=17.7\pm0.1;\gamma_{\langle T\rangle}=220.5\pm0.1)$. The black curve is Eq. (2).

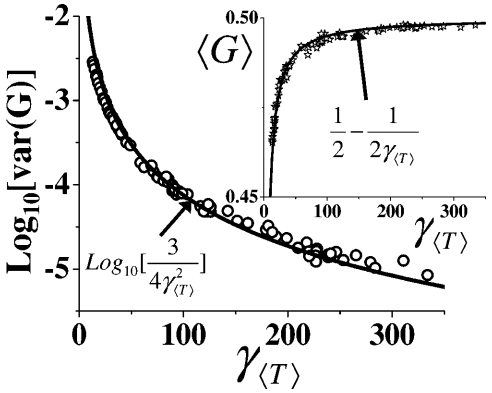

FIG. 5. The evolution of the variance of the experimentally determined $P(G;\gamma)$ distributions, i.e., var(G) (shown as the black circles) for increasing values of $\gamma_{\langle T\rangle}$ is plotted on a logarithmic scale. Inset: The evolution of the mean of the experimentally determined $P(G;\gamma)$ distributions, i.e., $\langle G\rangle$ (shown as the black stars) for increasing values of $\gamma_{\langle T\rangle}$ is shown. The solid black lines represent the leading terms in Eq. (3) and Eq. (4), and constitute zero-parameter fits.

V. TESTING PREDICTIONS FOR THE MEAN AND VARIANCE OF THE UCF PDFs

In Fig. 5, we again employ the sliding frequency window of width 1 GHz to test the asymptotic ($\gamma \gg 1$) relations for the mean $\langle G \rangle$ [Eq. (3)] and variance var(G) [Eq. (4)] of $P(G;\gamma)$ as a function of dephasing (loss) parameter γ. As before, we determine the value of $\gamma_{\langle T \rangle}$ for each frequency window data set that runs from 3 to 18 GHz for the three loss cases—0, 1, and 2. We then determine the corresponding values of the mean and variance of the corresponding conductance distributions $P(G;\gamma)$ of each frequency window. In the inset of Fig. 5, each black star indicates the experimentally estimated mean value of G (i.e., $\langle G \rangle$) for the corresponding value of $\gamma_{\langle T \rangle}$. The standard deviation about the experimentally determined mean is of the order 10^{-5}. We observe that as $\gamma_{\langle T \rangle}$ increases, the black stars asymptotically approach the classical value of $\langle G \rangle = 1/2$. The solid black curve represents the leading terms in Eq. (3).

The black circles in Fig. 5 show a similar analysis for the variance [var(G)] of the normalized conductance distributions $P(G;\gamma)$ as a function of γ. The solid black curve represents the leading term in Eq. (4). We observe that the black circles closely follow the functional approximation for the theoretical curve [Eq. (4)] for the range of $\gamma_{\langle T \rangle}$ values from about 18 to about 330, with no adjustable parameters.

VI. SUMMARY AND CONCLUSIONS

The results discussed in this paper provide experimental evidence in support of the theoretical arguments proposed by Ref. 15 and the hypothesis that random matrix theory provides a good description of the conductance fluctuation statistics in a ballistic chaotic quantum dot in the presence of dephasing. We have shown that in the "locally weak absorbing limit" as discussed in Ref. 15, the dephasing parameter can be related to the cavity loss parameter. We have derived an empirical linear relation between γ and the cavity loss-parameter $k^2/(\Delta k_n^2 Q)$ based on our experimental data. The finite conductivity of the metallic walls of the cavity translates to a minimum-possible experimentally accessible γ value of about 11 for our experiments (at least for the present cavity geometry and temperatures of −78.5 °C and above). We have shown that our experimentally determined conductance distributions and the asymptotic analytic functional forms for the PDF of G [$P(G)$], its mean value ($\langle G \rangle$) and variance [var(G)] are in good agreement over a broad range of large γ values. This also establishes the microwave analog as a method to study detailed theories of noninteracting quantum transport and decoherence in quantum coherent systems.

We acknowledge useful discussions with R. Prange and S. Fishman, as well as comments from P. Brouwer, P. Pereyra, and T. Seligman. This work is supported by the DoD MURI for the study of microwave effects under AFOSR Grant No. F496200110374, AFOSR DURIP Grants Nos. FA95500410295 and FA95500510240, and by the Israel/U.S.A. Binational Science Foundation.

[1] Y. Alhassid, Rev. Mod. Phys. **72**, 895 (2000).
[2] B. L. Altshuler and B. D. Simons, *Mesoscopic Quantum Physics*, edited by E. Akkermans, G. Montambaux, J.-L. Pichard, and J. Zinn-Justin (Elsevier, Amsterdam, 1995).
[3] P. A. Lee and A. D. Stone, Phys. Rev. Lett. **55**, 1622 (1985).
[4] A. G. Huibers, S. R. Patel, C. M. Marcus, P. W. Brouwer, C. I. Duruöz, and J. S. Harris, Jr., Phys. Rev. Lett. **81**, 1917 (1998).
[5] M. L. Mehta, *Random Matrices*, 3rd edition (Academic Press, New York, 2004).
[6] S. Washburn and R. A. Webb, Adv. Phys. **35**, 375 (1986).
[7] P. Mohanty and R. A. Webb, Phys. Rev. Lett. **88**, 146601 (2002).
[8] N. Agraït, A. L. Yeyati, and J. M. Ruitenbeek, Phys. Rep. **377**, 81 (2003); and references therein.
[9] E. Joos, H. D. Zeh, C. Kiefer, D. Giulini, J. Kupsch, and I. O. Stamatescu, *Decoherence and the Appearance of a Classical World in Quantum Theory* (Springer, Berlin, 1996).
[10] M. Büttiker, Phys. Rev. B **33**, 3020 (1986).
[11] H. U. Baranger, Phys. Rev. B **51**, 4703 (1995).
[12] A. G. Huibers, M. Switkes, C. M. Marcus, K. Campman, and A. C. Gossard, Phys. Rev. Lett. **81**, 200 (1998).
[13] K. B. Efetov, Phys. Rev. Lett. **74**, 2299 (1995).
[14] E. McCann and I. V. Lerner, J. Phys.: Condens. Matter **8**, 6719 (1996).
[15] P. W. Brouwer and C. W. J. Beenakker, Phys. Rev. B **55**, 4695 (1997).
[16] M. R. Zirnbauer, Nucl. Phys. A **560**, 95 (1993).
[17] C. H. Lewenkopf, A. Müller, and E. Doron, Phys. Rev. A **45**, 2635 (1992).
[18] X. Zheng, T. M. Antonsen, and E. Ott, Electromagnetics **26**, 3 (2006); X. Zheng, T. M. Antonsen, and E. Ott, *ibid.* **26**, 37 (2006).
[19] S. Hemmady, X. Zheng, E. Ott, T. M. Antonsen, and S. M. Anlage, Phys. Rev. Lett. **94**, 014102 (2005).
[20] S. Hemmady, X. Zheng, T. M. Antonsen, E. Ott, and S. M. Anlage, Phys. Rev. E **71**, 056215 (2005).
[21] S. Hemmady, X. Zheng, J. Hart, T. M. Antonsen, E. Ott, and S. M. Anlage, Phys. Rev. E **74**, 036213 (2006).
[22] E. Ott, *Chaos in Dynamical Systems* (Cambridge University Press, Cambridge, 1993).
[23] Y. H. Kim, M. Barth, H. J. Stockmann, and J. P. Bird, Phys. Rev. B **65**, 165317 (2002).
[24] H. J. Stöckmann, *Quantum Chaos—An Introduction* (Cambridge University Press, Cambridge, 1999).
[25] H. J. Stöckmann and J. Stein, Phys. Rev. Lett. **64**, 2215 (1990).
[26] H.-D. Gräf, H. L. Harney, H. Lengeler, C. H. Lewenkopf, C. Rangacharyulu, A. Richter, P. Schardt, and H. A. Weidenmüller, Phys. Rev. Lett. **69**, 1296 (1992).
[27] A. Kudrolli, S. Sridhar, A. Pandey, and R. Ramaswamy, Phys. Rev. E **49**, R11 (1994).
[28] S. Sridhar, Phys. Rev. Lett. **67**, 785 (1991).

[29] J. Stein and H. J. Stöckmann, Phys. Rev. Lett. **68**, 2867 (1992).
[30] D. H. Wu, J. S. A. Bridgewater, A. Gokirmak, and S. M. Anlage, Phys. Rev. Lett. **81**, 2890 (1998).
[31] A. Gokirmak, D.-H. Wu, J. S. A. Bridgewater, and S. M. Anlage, Rev. Sci. Instrum. **69**, 3410 (1998).
[32] S. H. Chung, A. Gokirmak, D. H. Wu, J. S. A. Bridgewater, E. Ott, T. M. Antonsen, and S. M. Anlage, Phys. Rev. Lett. **85**, 2482 (2000).
[33] U. Kuhl, M. Martínez-Mares, R. A. Méndez-Sánchez, and H. J. Stöckmann, Phys. Rev. Lett. **94**, 144101 (2005).
[34] R. A. Méndez-Sánchez, U. Kuhl, M. Barth, C. H. Lewenkopf, and H. J. Stöckmann, Phys. Rev. Lett. **91**, 174102 (2003).
[35] H. Schanze, H. J. Stöckmann, M. Martínez-Mares, and C. H. Lewenkopf, Phys. Rev. E **71**, 016223 (2005).
[36] O. Hul, O. Tymoshchuk, S. Bauch, P. M. Koch, and L. Sirko, J. Phys. A **38**, 10489 (2005).
[37] C. W. J. Beenakker, Rev. Mod. Phys. **69**, 731 (1997).
[38] Since the variance is sensitive to the presence of outliers in our data sets, which arise due to imperfect normalization or calibration errors, we exclude the outlying 1% of the data points while calculating the variance of experimental PDFs.
[39] M. Vraničar, M. Barth, G. Veble, M. Robnik, and H. J. Stöckmann, J. Phys. A **35**, 4929 (2002).